

Graphene-like optical light field and its interaction with two-level atomsV. E. Lembessis,^{1,*} Johannes Courtial,^{2,†} N. Radwell,² A. Selyem,² S. Franke-Arnold,² O. M. Aldossary,^{1,3} and M. Babiker⁴¹*Department of Physics and Astronomy, College of Science, King Saud University, Post Office Box 2455, Riyadh 11451, Saudi Arabia*²*SUPA, School of Physics and Astronomy, University of Glasgow, Glasgow G12 8QQ, United Kingdom*³*National Center for Applied Physics, KACST, Post Office Box 6086, Riyadh 11442, Saudi Arabia*⁴*Department of Physics, University of York, Heslington, York YO10 5DD, United Kingdom*

(Received 28 October 2015; published 21 December 2015)

The theoretical basis leading to the creation of a light field with a hexagonal honeycomb structure resembling graphene is considered along with its experimental realization and its interaction with atoms. It is argued that associated with such a light field is an optical dipole potential which leads to the diffraction of the atoms, but the details depend on whether the transverse spread of the atomic wave packet is larger than the transverse dimensions of the optical lattice (resonant Kapitza-Dirac effect) or smaller (optical Stern-Gerlach effect). Another effect in this context involves the creation of gauge fields due to the Berry phase acquired by the atom moving in the light field. The experimental realization of the light field with a honeycomb hexagonal structure is described using holographic methods and we proceed to explore the atom diffraction in the Kapitza-Dirac regime as well as the optical Stern-Gerlach regime, leading to momentum distributions with characteristic but different hexagonal structures. The artificial gauge fields too are shown to have the same hexagonal spatial structure and their magnitude can be significantly large. The effects are discussed with reference to typical parameters for the atoms and the fields.

DOI: [10.1103/PhysRevA.92.063833](https://doi.org/10.1103/PhysRevA.92.063833)

PACS number(s): 42.50.Ct, 03.75.Be, 42.50.Tx

I. INTRODUCTION

The mechanical effects of coherent light on matter have been widely studied in recent decades, following the realization of laser cooling and trapping, which led to unprecedented control of atomic motion, culminating in the realization of Bose-Einstein condensation [1]. One of the benefits of the detailed control of atom-light interaction lies in the possibility of performing quantum simulations [1] of condensed-matter systems, which do not lend themselves to fundamental investigation. This is specifically the case in the context of integer and fractional quantum Hall effects.

The physical basis of magnetic-field effects is the well-known Lorentz force exerted on an electric charge by a magnetic field. Atoms are electrically neutral, so if we wish to simulate effects involving light and matter we must somehow create artificial or synthetic magnetic fields. There are different ways of generating such fields: (a) by employing rapidly rotating trapped ultracold gases; (b) by rapidly rotating atoms in micro traps; (c) by laser imprinting Berry-type phases on atoms; and (d) by creating a laser-induced gauge field in an optical lattice [2].

The past decade has seen much work carried out on the creation of optical lattices which provide an excellent environment for the realization of strongly correlated systems. This property of optical lattices lies on the efficient, almost absolute controllability of the interaction, shape, and strength of the atom-atom interactions via Feshbach resonances, while effects such as electron-phonon interaction, which in the solid-state context can destroy the coherence, are absent [2]. Among the optical lattices of interest we focus here on the characteristic hexagonal honeycomb structure. Such an optical

lattice has been experimentally realized over two decades ago using three coplanar beams [3]. In the past decade, following the advent of graphene, this type of optical lattice has once again come into focus.

The generation of an optical graphene-like potential in which cold atoms become trapped is motivated by the fact that it represents a cold-atom analog of real graphene. The honeycomb optical dipole potential associated with the light field is an adjustable versatile physical platform for a number of physical effects that can be simulated and which are difficult to study in real graphene. For example, by varying the directions and intensities of the optical lattice beams, one can imbalance the tunneling rates between the different honeycomb sites. This makes the Dirac points move inside the Brillouin zone until they merge and disappear, leading to a topological metal-insulator transition. This situation could, in principle, be obtained in real graphene samples by stretching the layer, but this is not easy to achieve. There are also other physical phenomena including Feshbach resonances, quantum magnetism, Cooper pairing, and the Bardeen-Cooper-Schrieffer (BCS) superfluidity that can be simulated with such potentials. The study of the two-dimensional dynamics of ultracold atoms in a hexagonal lattice [4] has led to the reproduction of some of the most important features of graphene [5].

In this paper we discuss the experimental realization of the graphene-like optical lattice using holographic techniques. This is followed by consideration of the effects of the interaction of the atomic beam with the light field in terms of the momentum distribution of the diffracted atoms and the construction of the artificial gauge magnetic fields arising from a Berry-type phase acquired by an atom moving in the graphene-like light field, which to the best of our knowledge have never before been calculated for such types of fields. We explore the characteristics of the effects with reference to typical parameters for the atoms and fields.

*vlmpesis@ksu.edu.sa

†Johannes.Courtial@glasgow.ac.uk

The paper is organized as follows. In Sec. II we show how a honeycomb optical lattice can be experimentally created using holographic methods. In Sec. III we consider the interaction of a two-level atom with the honeycomb-like field and we set up the generalized optical Bloch equations (GOBE), which describe the translational motion of the atom. Sections IV and V deal with the solution of the GOBE in two different diffraction regimes, namely the Kapitza-Dirac and the Stern-Gerlach regimes. In Sec. VI we describe the details leading to the artificial gauge magnetic field that can be produced when the light field interacts with a two-level atom. Finally, Sec. VII contains comments and conclusions.

II. HOLOGRAPHIC CREATION OF AN OPTICAL GRAPHENE POTENTIAL

We have used holographic methods to create an optical graphene potential in the form of a light field whose transverse intensity cross section has maxima at positions corresponding to the locations of C atoms in a planar sheet of graphene, namely on the vertices of a hexagonal tiling. We consider a light field with a transverse cross section (in the x, y plane) for which the complex amplitude function has the form

$$u(x, y) = \sum_{j=1}^6 (-1)^j \exp \left[ik_T \left(x \cos \frac{2\pi j}{6} + y \sin \frac{2\pi j}{6} \right) \right]. \quad (1)$$

This is a superposition of 6 equally bright uniform plane waves, each with transverse wave number k_T and associated wavelength $\lambda_T = 2\pi/k_T$. The \mathbf{k} vectors lie on the vertices of a regular hexagon. The phase factors play an important role here in that neighboring plane waves have opposite signs (provided by the $(-1)^j$ factor). The transverse intensity cross section of this field, which is proportional to the modulus squared of $u(x, y)$, is shown in Fig. 1.

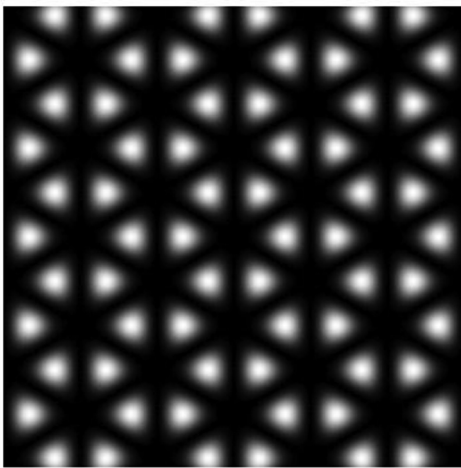


FIG. 1. Calculated transverse intensity distribution of a light field forming an optical graphene potential displayed on a square of side length $3\lambda_T$. The graph shows an intensity plot of the function $|u(x, y)|^2$. The intensity maxima are located on the vertices of hexagons, as in the structure of graphene. The graph is plotted for $k_T = 2\pi$, i.e., for $\lambda/\sin\theta = 1$, in the region $-3 \leq x, y \leq +3$.

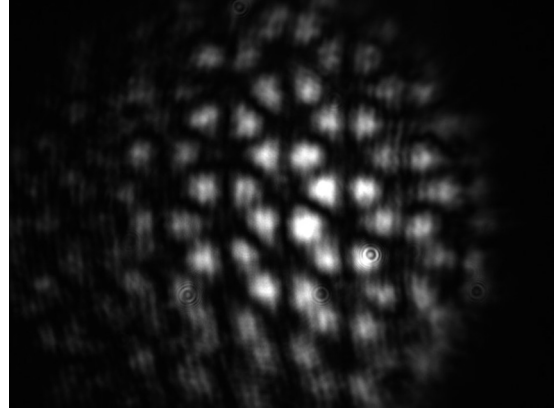


FIG. 2. Intensity cross section of the experimentally produced beam. The image represents a physical area of size $3.7 \text{ mm} \times 2.8 \text{ mm}$.

The method that we have adopted here works by creating, holographically, the field in the Fourier plane (i.e., the far field), and then Fourier transforming. In the Fourier plane, each plane wave is represented by a point, which we approximate with a small disk. The plane waves all have the same inclination angle with respect to the z axis, so that $k_z = k_{\parallel} = k \cos\theta$ and $k_T = k \sin\theta$, in our case $\theta = 0.11^\circ$. In k space, the plane waves lie on the vertices of a regular hexagon, centered on the k_z direction. The field pattern was created by shining the beam from a laser (homemade external-cavity diode laser, $\lambda = 780 \text{ nm}$), widened to a spot size $w \approx 2 \text{ mm}$ and collimated, onto a phase-only Spatial Light Modulator (Hamamatsu Liquid crystal on silicon) of size $\approx 16 \text{ mm} \times 12 \text{ mm}$ with 800×600 pixels, then through a Fourier lens ($f = 0.5 \text{ m}$), through an aperture in the Fourier lens's back focal plane that selected only the +1st diffraction order, and onto a Charge-coupled device (Allied Vision Tech GC660).

We note that the generated light field differs from that given in Eq. (1) as it originates from disks rather than points spaced around the vertices of a hexagon. This is necessary to increase efficiency, but results in a pattern with an intensity that is falling off rapidly around the beam waist, as shown in Fig. 2.

Figure 3 shows the hologram pattern. Ideally, to generate the field with the complex amplitude as given in Eq. (1), this would consist of 6 *points* that scatter light into the +1st diffraction order. To increase the efficiency, these points are actually *disks* with (more or less) uniform intensity distributions in the hologram plane. The resulting light field was therefore not the interference pattern due to six uniform plane waves; instead, it comprises six approximations to uniform plane waves whose superposition shows the hexagonal interference pattern of an optical graphene potential, but with the intensity of the pattern rapidly falling off towards the edge of the region. Figure 2 shows the intensity cross section of the resulting beam. Note that a superposition of uniform plane waves, all traveling at the same angle θ with respect to the z axis, is propagation invariant [6]. The beam produced is an approximation to such a superposition and should be approximately diffraction-free in some region of space. A monochromatic light beam with a cross section given by Eq. (1) is diffraction free, so there would be no traps in a plane. This means that the intensity is not very tightly confined (if at all) in the z direction to the maxima

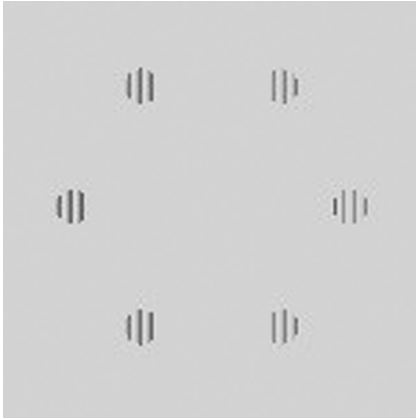


FIG. 3. The hologram pattern. Only the central 150×150 pixels of the hologram pattern are shown. The phase values (0 to 2π) are represented as gray level (black to white). The pattern consists of 6 spots, each of radius $125 \mu\text{m}$, centered on the vertices of a regular hexagon, 1 mm from the center of the hexagon. The phase difference between neighboring spots is π . The stripes across the spots send the light in those spots out at an angle; the beam at this angle forms the +1st diffraction order.

shown in Fig. 3. This could easily be changed by reflecting the beam back onto itself, which would give standing waves in the form of fringes in the z direction, separated by $\lambda_z/2$.

III. INTERACTION OF THE GRAPHENE-LIKE FIELD WITH TWO-LEVEL ATOMS

Consider the interaction of the field with a two-level atomic wave packet which has been chosen to propagate along the z axis, as shown in Fig. 4. We assume that the interaction time can be controlled by switching the light field on for a time interval $T \ll \Gamma^{-1}$ where Γ is the natural line width of the transition. We also suppose that the Doppler shift in this interaction is negligible compared with the natural width of the excited state, so $k_{\parallel}v_z \ll \Gamma$. An atom incident on the light field in the x - y plane is subject to interaction spanning a time interval $T \ll \Gamma^{-1}$ and thus experiences diffraction off the light field. A final assumption is that $k_T v_T \ll T^{-1}$, which means that we can neglect the spatial displacement of the atom in the x - y plane during the interaction time T , even if it experiences momentum changes by absorbing and emitting photons.

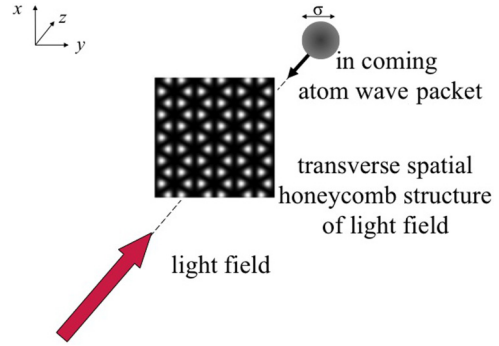


FIG. 4. (Color online) Schematic representation of the interaction of the two-level atoms with the light field. The atoms is considered as having a Gaussian transverse spatial distribution profile with a dispersion.

The interaction Hamiltonian has the following form:

$$H_{\text{int}}(x, y) = -\mathbf{d} \cdot \mathbf{E} = \mathbf{d} \cdot \mathbf{e} E_0 f(x, y) \cos(\omega t - k_{\parallel} z), \quad (2)$$

where \mathbf{e} is the field polarization vector, \mathbf{d} is the atomic dipole moment vector, E_0 is the field amplitude, and k_{\parallel} is the propagation wave vector along the z direction. The function $f(x, y)$ can be written as follows:

$$f(x, y) = -2 \sin\left(\frac{k_T x}{2} + \frac{k_T y \sqrt{3}}{2}\right) - 2 \sin\left(\frac{k_T x}{2} - \frac{k_T y \sqrt{3}}{2}\right) + 2 \sin(k_T x). \quad (3)$$

The Rabi frequency associated with the interaction of a two-level atom with the light field is given by

$$\Omega(x, y) = \Omega_0(x, y) f(x, y) \exp(ik_{\parallel} z), \quad (4)$$

where

$$\Omega_0 = -\frac{\mathbf{d} \cdot \mathbf{e}}{2\hbar} E_0. \quad (5)$$

We are now in a position to consider the diffraction of atoms off the graphene-like light field. The procedure requires as a first step specifying the generalized optical Bloch equations (GOBE) appropriate for the system since the quantum mechanical character of the gross motion of the atomic center of mass has to be taken into account. The details of this method have been given by Tanguy *et al.* in Ref. [7] and here we give a brief summary. The optical Bloch equations governing the diffraction are as follows:

$$\left(\frac{\partial}{\partial t} - \frac{i\hbar}{M} \frac{\partial^2}{\partial r \partial u}\right) \rho_{11}(\mathbf{r}, \mathbf{u}) = i\Omega\left(\mathbf{r} - \frac{\mathbf{u}}{2}\right) \rho_{12}(\mathbf{r}, \mathbf{u}) - i\Omega^*\left(\mathbf{r} + \frac{\mathbf{u}}{2}\right) \rho_{21}(\mathbf{r}, \mathbf{u}) + \Gamma \rho_{22}, \quad (6)$$

$$\left(\frac{\partial}{\partial t} - \frac{i\hbar}{M} \frac{\partial^2}{\partial r \partial u}\right) \rho_{21}(\mathbf{r}, \mathbf{u}) = \left[i(\omega - \omega_0) - \frac{1}{2}\Gamma\right] \rho_{21}(\mathbf{r}, \mathbf{u}) - i\Omega\left(\mathbf{r} + \frac{1}{2}\mathbf{u}\right) \rho_{11}(\mathbf{r}, \mathbf{u}) + i\Omega\left(\mathbf{r} - \frac{1}{2}\mathbf{u}\right) \rho_{22}(\mathbf{r}, \mathbf{u}), \quad (7)$$

$$\left(\frac{\partial}{\partial t} - \frac{i\hbar}{M} \frac{\partial^2}{\partial r \partial u}\right) \rho_{22}(\mathbf{r}, \mathbf{u}) = \left[-i(\omega - \omega_0) - \frac{1}{2}\Gamma\right] \rho_{22}(\mathbf{r}, \mathbf{u}) - i\Omega^*\left(\mathbf{r} + \frac{1}{2}\mathbf{u}\right) \rho_{21}(\mathbf{r}, \mathbf{u}) + i\Omega^*\left(\mathbf{r} - \frac{1}{2}\mathbf{u}\right) \rho_{11}(\mathbf{r}, \mathbf{u}). \quad (8)$$

Taking the Fourier transforms of Eqs. (6)–(8) with respect to \mathbf{u} we obtain the GOBE in the Wigner representation [8,9]. Working in a frame of reference coinciding with the atomic rest frame allows us to drop the free-flight terms in Eqs. (6)–(8) which describe the effect on the density matrix elements of the spatial displacement of the atom. This simplifies the analysis considerably [10]. Equations (6)–(8) then become strictly local in \mathbf{r} and \mathbf{u} ; i.e., they can be solved for each set (\mathbf{r}, \mathbf{u}) .

The relation between the functions which describe the ingoing and outgoing states is

$$F_{\text{out}}(\mathbf{p}, t) = \int d\mathbf{r} G(\mathbf{r}, \mathbf{p}, t) F_{\text{in}}(\mathbf{r}), \quad (9)$$

where the function $G(\mathbf{r}, \mathbf{p}, T)$ is given by

$$G(\mathbf{r}, \mathbf{p}, T) = \frac{1}{\hbar^3} \int d^3u L(\mathbf{r}, \mathbf{u}, T) \exp(-i\mathbf{p} \cdot \mathbf{u}/\hbar). \quad (10)$$

The function $L(\mathbf{r}, \mathbf{u}, T)$ is the inverse Laplace transform, which can be written as follows:

$$L(\mathbf{r}, \mathbf{u}, s) = P_3(s)/P_4(s), \quad (11)$$

where P_3 and P_4 are polynomials of degree three and four in s with coefficients depending on \mathbf{r} and \mathbf{u} . In the case of short time limit (i.e., time intervals $T \ll \Gamma^{-1}$) we can neglect terms proportional to Γ and these polynomials then have the form

$$P_3(s) = 2s\Omega(\mathbf{r} + \frac{1}{2}\mathbf{u})\Omega^*(\mathbf{r} - \frac{1}{2}\mathbf{u}) + s^3 + s[|\Omega(\mathbf{r} + \frac{1}{2}\mathbf{u})|^2 + |\Omega(\mathbf{r} - \frac{1}{2}\mathbf{u})|^2], \quad (12)$$

$$P_4(s) = s^4 + 2s^2[|\Omega(\mathbf{r} + \frac{1}{2}\mathbf{u})|^2 - |\Omega(\mathbf{r} - \frac{1}{2}\mathbf{u})|^2] + [|\Omega(\mathbf{r} + \frac{1}{2}\mathbf{u})|^2 - |\Omega(\mathbf{r} - \frac{1}{2}\mathbf{u})|^2]^2, \quad (13)$$

where

$$\Omega(\mathbf{r} + \frac{1}{2}\mathbf{u}) = U_1 \exp(ik_{\parallel}z + ik_{\parallel}u_z/2), \quad (14)$$

$$\Omega(\mathbf{r} - \frac{1}{2}\mathbf{u}) = U_2 \exp(ik_{\parallel}z - ik_{\parallel}u_z/2), \quad (15)$$

and

$$U_1 = \Omega_0 \left[\sin\left(k_T x + \frac{k_T u_x}{2}\right) - 2 \sin\left(\frac{k_T x}{2} + \frac{k_T u_x}{4}\right) \times \sin\left(\frac{k_T y \sqrt{3}}{2} + \frac{k_T u_y \sqrt{3}}{4}\right) \right], \quad (16)$$

$$U_2 = \Omega_0 \left[\sin\left(k_T x - \frac{k_T u_x}{2}\right) - 2 \sin\left(\frac{k_T x}{2} - \frac{k_T u_x}{4}\right) \times \sin\left(\frac{k_T y \sqrt{3}}{2} - \frac{k_T u_y \sqrt{3}}{4}\right) \right]. \quad (17)$$

These enable $L(\mathbf{r}, \mathbf{u}, T)$ to be written in the following form:

$$L(\mathbf{r}, \mathbf{u}, T) = \cos[T(U_1 - U_2)/2][1 + \exp(ik_{\parallel}u_z)] + \cos[T(U_1 + U_2)/2][1 - \exp(ik_{\parallel}u_z)]. \quad (18)$$

In the following we discuss two different cases of the atomic diffraction depending on whether the transverse spread of the atomic wave packet is larger than the transverse dimensions of the optical lattice (resonant Kapitza-Dirac effect) or smaller (optical Stern-Gerlach).

IV. RESONANT KAPITZA-DIRAC EFFECT

We assume that the atomic system is described by a wave packet with spatial distribution $F_{\text{in}}(x, y, z) = \Psi(z)R(x, y) \exp(iP_z z/\hbar)$, i.e., prior to entering the field region. The atoms are assumed to be released from a trap and then accelerated by gravity to gain momentum P_z . The atomic wave packet is assumed to have a transverse width much larger than k_T^{-1} . After interaction with the field, the momentum distribution of the atoms is described by $F_{\text{out}}(\mathbf{p})$, which is given by

$$F_{\text{out}}(\mathbf{p}) = \int dx dy G(x, y, \mathbf{p}, t) F_{\text{in}}(x, y, z). \quad (19)$$

It can be shown that $U_1 \pm U_2$ appearing in Eq. (18) are as follows. For $U_1 - U_2$ we have

$$U_1 - U_2 = \Omega_0 \left[A_- \sin\left(\frac{k_T u_x}{2}\right) + B_- \sin\left(\frac{k_T u_x}{4} + \frac{k_T u_y \sqrt{3}}{4}\right) + C_- \sin\left(\frac{k_T u_x}{4} - \frac{k_T u_y \sqrt{3}}{4}\right) \right] \quad (20)$$

with

$$A_- = -2 \cos(k_T x) \quad (21)$$

$$B_- = -2 \cos\left(\frac{k_T x}{2} + \frac{k_T y \sqrt{3}}{2}\right), \quad (22)$$

$$C_- = -2 \cos\left(\frac{k_T x}{2} - \frac{k_T y \sqrt{3}}{2}\right), \quad (23)$$

while for $U_1 + U_2$ we have

$$U_1 + U_2 = \Omega_0 \left[A_+ \cos\left(\frac{k_T u_x}{2}\right) + B_+ \cos\left(\frac{k_T u_x}{4} + \frac{k_T u_y \sqrt{3}}{4}\right) + C_+ \cos\left(\frac{k_T u_x}{4} - \frac{k_T u_y \sqrt{3}}{4}\right) \right] \quad (24)$$

with

$$A_+ = -2 \sin(k_T x), \quad (25)$$

$$B_+ = 2 \cos\left(\frac{k_T x}{2} + \frac{k_T y \sqrt{3}}{2}\right), \quad (26)$$

$$C_+ = -2 \cos\left(\frac{k_T x}{2} - \frac{k_T y \sqrt{3}}{2}\right). \quad (27)$$

It is easily seen that $B_+ = -B_-$ and $C_+ = C_-$. The expression for the propagator emerges in the following form:

$$G(x, y, \mathbf{p}, T) = \delta\left(P_x - \frac{\hbar k_T(m-l-2n)}{4}\right) \delta\left(P_y - \frac{\hbar k_T(m-l)\sqrt{3}}{4}\right) [(R_{nlm} - R_{n'l'm'})\delta(P_z - \hbar k_{\parallel}) + (R_{nlm} + R_{n'l'm'})\delta(P_z)], \quad (28)$$

where

$$R_{nlm} = \frac{1}{2} \sum_{n,m,l=-\infty}^{\infty} \left[J_n \left(\frac{\Omega_0 T A_-}{2} \right) J_m \left(\frac{\Omega_0 T B_-}{2} \right) J_l \left(\frac{\Omega_0 T C_-}{2} \right) + J_{-n} \left(\frac{\Omega_0 T A_-}{2} \right) J_{-m} \left(\frac{\Omega_0 T B_-}{2} \right) J_{-l} \left(\frac{\Omega_0 T C_-}{2} \right) \right] \quad (29)$$

$$R_{n'l'm'} = \frac{1}{2} \sum_{n',m',l'=-\infty}^{\infty} (1 + i^{(m'+l')}) \left[J_{n'} \left(\frac{\Omega_0 T A_+}{2} \right) J_{m'} \left(\frac{\Omega_0 T B_+}{2} \right) J_{l'} \left(\frac{\Omega_0 T C_+}{2} \right) + J_{-n'} \left(\frac{\Omega_0 T A_+}{2} \right) J_{-m'} \left(\frac{\Omega_0 T B_+}{2} \right) J_{-l'} \left(\frac{\Omega_0 T C_+}{2} \right) \right]. \quad (30)$$

The expression for $G(x, y, P_x, P_y, T)$ shows that the propagator is a comb of δ functions which exhibits a hexagonal structure in momentum space. This structure originates from the redistribution of photons between the different plane waves which constitute our light-field configuration.

We suppose that the incoming wave packets have a width along the x - y plane much larger than the wavelength of the light. Also we assume that initial momentum of the atom in the z direction is larger than the photon momentum kick in this direction. Simultaneously, as discussed in Sec. III, the Doppler shift does not exceed Γ . To explore whether these two conditions are compatible we consider the following example. We consider the transition $5^2S_{1/2} - 5^2P_{3/2}$ of ^{85}Rb atoms for which $\Gamma = 3.25 \times 10^7$ Hz. To excite this transition our light field must have a wavelength equal to 780 nm. The absorption of a photon imparts a recoil velocity to the atom equal to 5.4×10^{-3} m/s. This means that the atom velocities are limited to the range $v_{\parallel} < 4.41$ m/s. So our analysis holds

for velocities in the region 5.4×10^{-3} m/s $< v_{\parallel} < 4.41$ m/s. Thus, we can assume that in the momentum distribution of the scattered atoms we have $\delta(P_z - \hbar k_{\parallel}) \approx \delta(P_z)$, in which case we can write

$$G(x, y, \mathbf{p}, T) = 2R_{nlm} \delta \left(P_x - \frac{\hbar k_T (m - l - 2n)}{4} \right) \times \delta \left(P_y - \frac{\hbar k_T (m - l) \sqrt{3}}{4} \right) \delta(P_z). \quad (31)$$

The scattered atomic distribution can then be written as

$$F_{\text{out}}(p) = \delta(P_z) \int_{-2\lambda/3}^{+2\lambda/3} dx \int_{-\sqrt{3}\lambda/3}^{+\sqrt{3}\lambda/3} dy R(x, y) G(x, y, \mathbf{p}, T). \quad (32)$$

By substituting in Eq. (31) for $G(x, y, \mathbf{p}, T)$ as given in Eq. (28) we can then write

$$F_{\text{out}}(p) = \delta(P_z) \sum_{n=-\infty}^{\infty} \sum_{m=-\infty}^{\infty} \sum_{l=-\infty}^{\infty} \delta \left(P_x - \frac{\hbar k_T (m - l - 2n)}{4} \right) \delta \left(P_y - \frac{\hbar k_T (m - l) \sqrt{3}}{4} \right) \times \int_{-2\lambda/3}^{+2\lambda/3} dx \int_{-\sqrt{3}\lambda/3}^{+\sqrt{3}\lambda/3} dy R(x, y) \{ [1 + (-1)^{n+l+m}] J_n(\Omega_0 T A) J_m(\Omega_0 T B) J_l(\Omega_0 T C) \}, \quad (33)$$

where $\lambda = 2\pi/k_T$ and the integrals involving the Bessel functions determine the strength of the diffraction pattern. The integrations span the limits of a hexagonal cell of the electric field given in Eqs. (2) and (3). We have assumed that the incoming atomic wave packet has a width along x and y directions much larger than the laser light periodicity. The integral is in principle defined on this whole width. As the incoming atomic spatial distribution varies very slowly with x and y and $G(x, y, T)$ is a periodic function of x and y the integrals in Eqs. (32) and (33) are within these limits [11]. The terms which survive in the infinite series are those for which the sum $n + l + m$ is an even number which leads to a restriction on the diffraction terms $(m - l - 2n)$ and $(m - l)$ appearing in the δ functions. For example, the central part of the diffraction pattern corresponds to $(m - l - 2n) = 0$ and $(m - l) = 0$, which means that $n = 0$ and so l and m such that the sum $l + m$ is an even number. Similarly we cannot have in the diffraction pattern the orders $(m - l - 2n, m - l) = (1, 0), (0, 1), (1, 1), (0, 2), (0, -2)$ but we can have the order $(m - l - 2n, m - l) = (2, 2)$ etc. Once we specify the wave function of the incoming atoms we can employ numerical techniques.

For instance, consider a Gaussian transverse atomic wave function given by $R(x, y) = (2\sqrt{\ln 2}/\sigma\sqrt{\pi}) \exp(-4 \ln 2(x^2 + y^2)/\sigma^2)$ where σ is the transverse size of the wave packet which, for a typical BEC experiment [12], can take the value of $\sigma = 21 \mu\text{m}$. In this case the central diffraction spot which corresponds to $(n, l, m) = (0, 0, 0)$ is found to amount to a value equal to 0.196. The distribution given in Eq. (33) shows the physical basis of the diffraction of the atomic wave packet which results from the redistribution of photons between the plane wave beams that they have been interfered to correspond to the total light field given in Eq. (1). The atom may absorb one photon from the one plane wave and emit it into another. We can understand this better with a qualitative discussion of the interaction of the light field with the atom. The function $f(x, y)$ which characterizes the interaction and is given in Eq. (3) contains sin terms which can be expressed in terms of the complex exponentials $\exp(\pm i \mathbf{k} \cdot \mathbf{r})$, with \mathbf{k} being $\mathbf{k}_0 = k_T \hat{\mathbf{x}}$, $\mathbf{k}_+ = k_T(\hat{\mathbf{x}}/2 + \sqrt{3}\hat{\mathbf{y}}/2)$ or $\mathbf{k}_- = k_T(\hat{\mathbf{x}}/2 - \sqrt{3}\hat{\mathbf{y}}/2)$. The relation $\exp(\pm i \mathbf{k} \cdot \mathbf{r}) = \sum_{\mathbf{p} \pm \hbar \mathbf{k}} \langle \mathbf{p} \rangle$ applied to each of the vectors \mathbf{k}_0 , \mathbf{k}_+ , and \mathbf{k}_- indicates that the interaction couples actually the atomic momentum to integer multiples of the

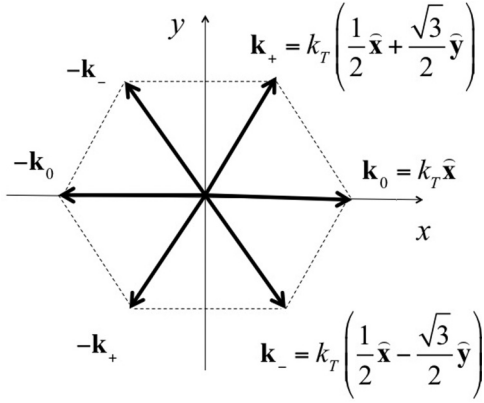


FIG. 5. Schematic representation of the momentum exchange between the two-level atoms and the light field.

momenta $\pm \hbar \mathbf{k}_0$, $\pm \hbar \mathbf{k}_+$ and $\pm \hbar \mathbf{k}_-$. Figure 5 shows that the tips of these momentum vectors form a hexagon.

V. OPTICAL STERN-GERLACH EFFECT

The second regime of interest is when the spatial extent of the atomic wave packet is smaller than the optical wavelength (i.e., $k_T u \ll 1$ in the OBEs). In this case we may make the following approximations for the relevant expressions appearing in Eq. (21):

$$\begin{aligned} \sin\left(\frac{k_T u_x}{2}\right) &\approx \frac{k_T u_x}{2} \\ \sin\left(\frac{k_T u_x}{4} \pm \frac{k_T u_y \sqrt{3}}{4}\right) &\approx \frac{k_T u_x}{4} \pm \frac{k_T u_y \sqrt{3}}{4}. \end{aligned} \quad (34)$$

The corresponding cosine terms in Eq. (25) can be set as approximately equal to 1. The above approximations give the following form to Eqs. (20) and (24):

$$\begin{aligned} U_1 - U_2 &= \Omega_0 \left[\left(\frac{A_-}{2} + \frac{B_-}{4} + \frac{C_-}{4} \right) k_T u_x \right. \\ &\quad \left. + \left(\frac{B_-}{4} + \frac{C_-}{4} \right) k_T u_y \sqrt{3} \right], \end{aligned} \quad (35)$$

$$U_1 + U_2 = \Omega_0 (A_+ + B_+ + C_+). \quad (36)$$

The corresponding $G(x, y, q_x, q_y, T)$ is now as follows:

$$\begin{aligned} G(x, y, q, p, T) &= [\delta(q_x + A_x) \delta(q_y + A_y) \\ &\quad + \delta(q_x - A_x) \delta(q_y - A_y)] [\delta(P_z) + \delta(P_z - \hbar k_{||})] \\ &\quad + \cos(A_z) \delta(q_x) \delta(q_y) [\delta(P_z) - \delta(P_z - \hbar k_{||})], \end{aligned} \quad (37)$$

where A_x , A_y , and A_z are given by

$$A_x = \frac{\Omega_0 T k_T}{2} \left(\frac{A_-}{2} + \frac{B_-}{4} + \frac{C_-}{4} \right), \quad (38)$$

$$A_y = \frac{\Omega_0 T k_T \sqrt{3}}{2} \left(\frac{B_-}{4} + \frac{C_-}{4} \right), \quad (39)$$

$$A_z = \frac{\Omega_0 T}{2} (A_+ + B_+ + C_+). \quad (40)$$

Once more, if we are in the atom rest frame, Eq. (37) assumes a simpler form if the atom momentum P_z is much larger than the momentum $\hbar k_{||}$ delivered by the photon in the beam propagation direction, in which case Eq. (37) becomes

$$\begin{aligned} G(x, y, q_x, q_y, T) &= [\delta(q_x + A_x) \delta(q_y + A_y) \\ &\quad + \delta(q_x - A_x) \delta(q_y - A_y)] \delta(P_z). \end{aligned} \quad (41)$$

In the case where the spatial extent of the atomic wave packet is smaller than the optical wavelength it can be shown [7] that the outgoing atom momentum distribution is given by

$$F_{\text{out}}(\mathbf{p}) = \int dq_x dq_y G(x_0, y_0, T) F_{\text{in}}(P_x - q_x, P_y - q_y), \quad (42)$$

where (x_0, y_0) are the coordinates of the point where the narrow wave packet crosses the light field. By inserting in the above relation Eq. (41), we get the atomic momentum distribution, which is given by

$$\begin{aligned} F_{\text{out}}(\mathbf{p}) &= F_{\text{in}}[P_x - A_x(x_0, y_0), P_y - A_y(x_0, y_0)] \\ &\quad + F_{\text{in}}[P_x + A_x(x_0, y_0), P_y + A_y(x_0, y_0)]. \end{aligned} \quad (43)$$

For example, when the atom crosses the field at the point $(x_0, y_0) = (0, 0)$ then it is easy to show that $A_- = B_- = C_- = -2$ and thus $A_x = -\Omega_0 T k_T$ and $A_y = -\sqrt{3} \Omega_0 T k_T / 2$.

We see that in this case the final atomic distribution consists of two parts. This is a result of the fact that the transverse dimensions of the atomic wave packet are small compared with the period of the potential; in other words the atom is well localized in space. The atom, then, sees a local potential and splits in two parts which are π out of phase with each other. The mean transverse positions of these two wave packets perform oscillations on the x - y plane [13].

VI. ARTIFICIAL MAGNETIC FIELD IN THE GRAPHENE-LIKE LIGHT FIELD

It has been established that the gross motion of an electrically neutral atom moving in a laser field mimics the dynamics of a charged particle in a magnetic field as a result of the action of a Lorentz-like force [14]. This is a consequence of the Aharonov-Bohm phase acquired by the particle when it travels along a closed path C [15]. This phase is geometrical in nature since it does not depend on the duration needed to complete the trajectory. Thus in order to exhibit artificial magnetism, we must find a situation where a neutral particle acquires a geometrical phase when it moves along a closed path. To achieve this, we exploit the Berry phase effect in atom-light interactions [16, 17] where the coupling is represented by atomic dressed states [18], which can vary on a short spatial scale (typically of the order of the wavelength of light) and the artificial gauge fields can be quite strong. We assume that the atomic system at time $t = 0$ is prepared in a dressed state $|\chi(\mathbf{r}_0(t))\rangle$ and moves slowly enough that it follows adiabatically the local dressed state $|\chi(\mathbf{r}_0(t))\rangle$. When the atom completes the trajectory C it returns to the dressed state $|\chi(\mathbf{r}_0(t))\rangle$ having acquired a phase factor which contains a geometric component. The quantum motion of the atom is formally equivalent to that of a charged particle in a static magnetic field. Such models have been studied for two-level

atoms as well as for three-level atoms in different beam configurations [14,19].

Here we consider the atom as a two-level system with a transition frequency ω_0 . It is well established [1] that the interaction of the two-level atom with a coherent light field gives rise to two dressed states, namely

$$|\chi(\mathbf{r}_1(t))\rangle = \begin{pmatrix} \cos[\Theta(\mathbf{R}/2)] \\ \exp[i\phi(\mathbf{R})] \sin[\Theta(\mathbf{R}/2)] \end{pmatrix}, \quad (44)$$

$$|\chi(\mathbf{r}_2(t))\rangle = \begin{pmatrix} -\exp[i\phi(\mathbf{R})] \sin[\Theta(\mathbf{R}/2)] \\ \cos[\Theta(\mathbf{R}/2)] \end{pmatrix}, \quad (45)$$

with ϕ the position-dependent phase of the field and

$$\cos[\Theta(\mathbf{R})] = \frac{\delta}{\sqrt{\delta^2 + \Omega^2(\mathbf{R})}}. \quad (46)$$

Here δ is the detuning of the atomic transition from the frequency of the light and $\Omega(\mathbf{R})$ is the Rabi frequency given in Eq. (4). As has been shown [18], under adiabaticity conditions we now have an artificial magnetic field given by

$$q\mathbf{B}(\mathbf{R}) = -\hbar\delta \frac{\Omega(\mathbf{R})}{[\delta^2 + \Omega^2(\mathbf{R})]^{3/2}} \vec{\nabla}[\Omega(\mathbf{R})] \times \vec{\nabla}[\phi(\mathbf{R})]. \quad (47)$$

In our case the phase of the field is $-k_{\parallel}z$ so the gradient of the phase and the Rabi frequency are given respectively by

$$\vec{\nabla}[\phi(\mathbf{R})] = -k_{\parallel}\mathbf{z}, \quad (48)$$

$$\vec{\nabla}[\Omega(\mathbf{R})] = \Omega_0 \vec{\nabla}[f(x,y)] = \Omega_0 \left(\frac{\partial f}{\partial x} \mathbf{i} + \frac{\partial f}{\partial y} \mathbf{j} \right), \quad (49)$$

with

$$\frac{\partial f}{\partial x} = k_T \left[\cos\left(\frac{k_T x}{2} + \frac{k_T y \sqrt{3}}{2}\right) - \cos\left(\frac{k_T x}{2} - \frac{k_T y \sqrt{3}}{2}\right) + 2 \cos(k_T x) \right], \quad (50)$$

$$\frac{\partial f}{\partial y} = \frac{k_T \sqrt{3}}{2} \left[-\cos\left(\frac{k_T x}{2} + \frac{k_T y \sqrt{3}}{2}\right) + \cos\left(\frac{k_T x}{2} - \frac{k_T y \sqrt{3}}{2}\right) \right]. \quad (51)$$

From Eq. (47) we get an artificial gauge field with components along x and y directions. We now consider the case where our light field can excite the $5^2S_{1/2} - 5^2P_{3/2}$ transition in a ^{85}Rb atom which has an excited state spontaneous rate $\Gamma = 3.25 \times 10^7$ Hz. Our light field has a wavelength equal to 780 nm. We assume a detuning $\delta = \sqrt{2}\Gamma$, a Rabi frequency $\Omega_0 = 3\Gamma$, and a tilting angle $\theta = 20^\circ$. The resulting artificial magnetic field has two components, B_x and B_y , which are presented in Figs. 6 and 7.

These figures show clearly the hexagonal structure of the magnetic field components. Their relative size is quite large. If the fields act on an electric charge equal to the charge of electron, then, as the figures show, we have created artificial fields of the order of few tenths of T, which are much larger than those of the order of mT demonstrated elsewhere [20].

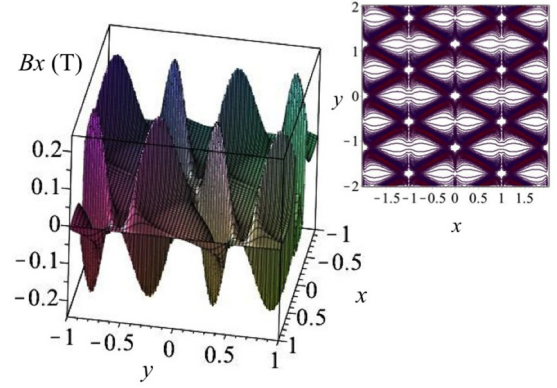


FIG. 6. (Color online) The artificial magnetic field component along the x direction. The units are in Tesla if we consider simulation of the motion of a particle having the charge of an electron. In the inset the corresponding contour plot. The distances in the x and y directions are scaled in wavelength λ units.

The characteristic features of this artificial field is its staggered form with sharp spatial gradients.

The theory of artificial gauge fields also predicts the existence of a scalar potential which is given by the following relation:

$$W(\mathbf{R}) = \frac{\hbar^2}{2M} \{ \vec{\nabla}[\Theta(\mathbf{R})]^2 + \sin^2[\Theta(\mathbf{R})] [\vec{\nabla}\phi(\mathbf{R})]^2 \}. \quad (52)$$

After further manipulations this scalar potential reduces to the following expression:

$$W(\mathbf{R}) = \frac{\hbar^2}{2M} \left\{ \frac{\delta^2}{(\delta^2 + \Omega^2)^2} [\vec{\nabla}\Omega(\mathbf{R})]^2 + \frac{\Omega^2}{\delta^2 + \Omega^2} [\vec{\nabla}\phi(\mathbf{R})]^2 \right\}. \quad (53)$$

From Eq. (53) we see that the scalar potential $W(\mathbf{R})$ is made up of two terms: one proportional to $[\vec{\nabla}\Omega(\mathbf{R})]^2$ which will result in a factor k_T^2 while the second term is proportional to $[\vec{\nabla}\phi(\mathbf{R})]^2$ and will result in a factor k_{\parallel}^2 and so it is easy to see

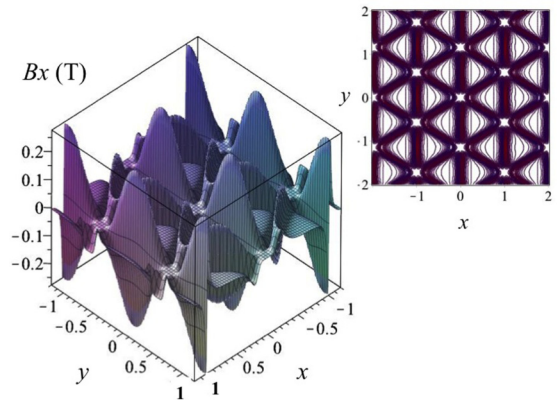


FIG. 7. (Color online) The artificial magnetic field component along the y direction. The units are in Tesla if we consider simulation of the motion of a particle having the charge of an electron. In the inset the corresponding contour plot. The distances in the x and y directions are scaled in wavelength λ units.

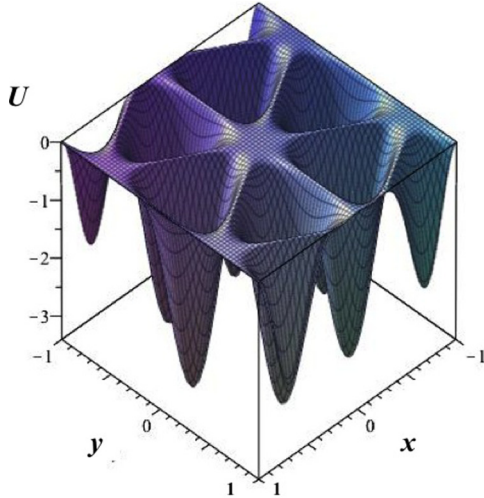


FIG. 8. (Color online) The optical dipole potential in atomic recoil energy units. The distances in the x and y directions are scaled in wavelength λ units.

that the second term is the dominant one. The scalar potential can be compared to the optical dipole trapping potential. It has been pointed out that the scalar potential can be comparable to the optical dipole potential once the detuning is sufficiently small [14]. For the parameters we used above in the plots for the artificial vector potential the scalar field is very small. For illustration we consider the case where $\Omega_0 = 0.07\Gamma$ and $\delta = 0.04\Gamma$ which lead to the Figs. 8 and 9 for the optical dipole and scalar potentials expressed in atom recoil energy units.

We see clearly that both exhibit a hexagonal structure but the scalar potential has large flat regions which means that it has a constant value and will change the potential felt by the atom, resulting in the distortions of the atomic cloud trapped in the potential. We see that the size of the artificial scalar field is about 30% of the depth of the optical dipole potential which can be as small as 1–2 recoil energies [21]. We have plotted the dipole potential for a negative detuning ($\omega_L < \omega_0$) which ensures a trapping at points of maximum intensity. For a positive detuning the possible trapping sites are actually saddle points and cannot ensure trapping. As our numerical work has shown the magnitude of these artificial fields can be varied significantly by adjusting the inclination angle of the waves interfering to compose our light field. Theoretically the upper limit of this inclination is 90 deg, which can (in principle) be achieved with extreme imaging through an infinitely large lens. The angle can very easily be increased to larger values by imaging with finite-size lenses that can be found in a typical laboratory. The above theory, both for vector and scalar fields, is valid provided $\hbar\Omega_0 \gg E_R$, where E_R is the atom recoil kinetic energy, a condition which is fully satisfied for the parameters we have used in the above numerical examples.

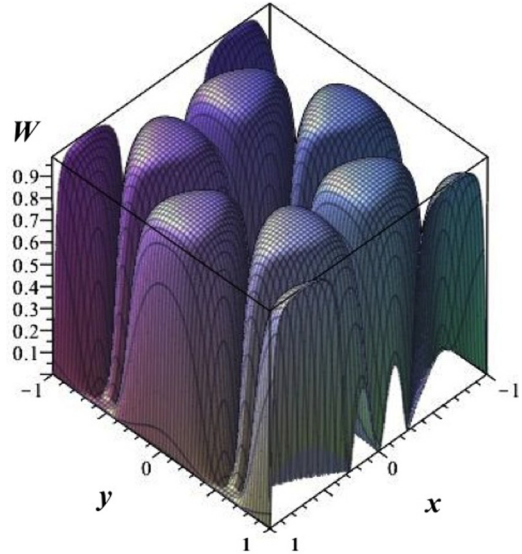


FIG. 9. (Color online) The scalar artificial gauge potential in atomic recoil energy units. The distances in the x and y directions are scaled in wavelength λ units.

VII. CONCLUSIONS

We have described the experimental generation of a coherent light field which has a transverse intensity pattern with a honeycomb structure. The creation of the field is achieved using phase-only Fourier holography, creating, approximately, a simple plane-wave superposition. We explored in some detail two scenarios involving the short-time interaction of two-level atoms with such a light field. First the diffraction of the atoms where the outgoing atomic momentum distribution are shown to exhibit a hexagonal structure reminiscent of the diffraction of x rays from an ordered crystal. Just as the outgoing x-ray spectrum reveals the structure of the crystal, the atomic momentum distribution after the diffraction reveals the structure of the diffracting light field. Second, we investigated the existence of artificial vector and scalar fields created by the interaction of the field with a two-level atom since our light field is characterized by strong amplitude and phase spatial gradients. We have provided numerical estimates of the gauge fields and demonstrated that the generated fields can have considerably large magnitudes.

ACKNOWLEDGMENTS

We thank Prof. C. Cohen-Tannoudji and Prof. S. Reynaud for clarifications and explanations on the methods used. We also thank Prof. I. Bloch for useful information on optical lattices potential depth. This Project was funded by the National Plan for Science, Technology and Innovation (MAARIFAH), King Abdulaziz City for Science and Technology, Kingdom of Saudi Arabia, Award No. (11-MAT1898-02).

- [1] C. Cohen-Tannoudji and D. Guery-Odelin, *Advances in Atomic Physics: An Overview* (World Scientific, Singapore, 2011).
 [2] M. Lewenstein, A. Sanpera, and V. Ahufinger, *Ultracold Atoms in Optical Lattices: Simulating Quantum Many Body Systems* (Oxford University Press, Oxford, UK, 2012).

- [3] G. Grynberg, B. Lounis, P. Verkerk, J.-Y. Courtois, and C. Salomon, *Phys. Rev. Lett.* **70**, 2249 (1993).
 [4] M. Snoek and W. Hofstetter, *Phys. Rev. A* **76**, 051603 (2007).
 [5] K. L. Lee, B. Gremaud, R. Han, B.-G. Englert, and C. Miniatura, *Phys. Rev. A* **80**, 043411 (2009).

- [6] J. Durnin, J. J. Miceli Jr., and J. H. Eberly, *Phys. Rev. Lett.* **58**, 1499 (1987).
- [7] C. Tanguy, S. Reynaud, and C. Cohen-Tannoudji, *J. Phys. B* **17**, 4623 (1984).
- [8] V. S. Letokhov and V. G. Minogin, *Phys. Rep.* **73**, 1 (1985).
- [9] J. Javainen and S. Stenholm, *Appl. Phys.* **21**, 163 (1980).
- [10] C. Tanguy, These de 3eme cycle, Paris XI (1983).
- [11] C. Cohen-Tannoudji and S. Reynaud (private communication).
- [12] M. F. Andersen, C. Ryu, P. Cladé, V. Natarajan, A. Vasiri, K. Helmerson, and W. D. Phillips, *Phys. Rev. Lett.* **97**, 170406 (2006).
- [13] P. Meystre, *Atom Optics* (Springer, New York, 2001).
- [14] J. Dalibard, F. Gerbier, G. Juzeliunas, and P. Öhberg, *Rev. Mod. Phys.* **83**, 1523 (2011).
- [15] M. V. Berry, *Proc. R. Soc. A* **392**, 45 (1984).
- [16] R. Dum and M. Olshanii, *Phys. Rev. Lett.* **76**, 1788 (1996).
- [17] P. M. Visser and G. Nienhuis, *Phys. Rev. A* **57**, 4581 (1998).
- [18] C. Cohen-Tannoudji, *Atoms in Electromagnetic Fields* (World Scientific, Singapore, 1994).
- [19] V. E. Lembessis, *J. Opt. Soc. Am. B* **31**, 1322 (2014).
- [20] G. Juzeliunas and P. Öhberg, in *Structured Light and Its Applications*, edited by D. L. Andrews (Elsevier, Burlington, MA, 2008).
- [21] I. Bloch (private communication).